Offset Vertical Radar Profiling

Alan Witten, School of Geology and Geophysics, University of Oklahoma, Norman, OK

John Lane, U.S. Geological survey, Office of Ground Water, Branch of Geophysics, Storrs, CT

Microbial digestion of organic contaminants is an in situ means for bio remediation that is currently under development and evaluation. Vegetable oil has been proposed as an agent to stimulate the natural microbial community. This system becomes anaerobic as the vegetable oil is consumed providing the necessary conditions for metabolizing volatile organic compounds (VOCs). In order for this process to be effective in remediating groundwater contamination, the vegetable oil must be introduced into contamination either directly or by creating a "curtain" down gradient.

There are several ways in which such a remediation can fail. One of these is that the vegetable oil stimulant does reach the desired area. As part of a larger program to evaluate the efficacy of the above-cited form of in situ bio remediation, geophysical techniques were employed to remotely characterize the spatial distribution of vegetable oil injected into a shallow unconfined area. The site is a riverfront park on the eastern bank of the Mississippi River and immediately down gradient of known VOC contamination. Approximately 100 m from the river a closely space cluster of wells was developed. Three inline wells were used for vegetable oil injection and approximately 13,700 liters of vegetable/groundwater mix was introduced into these wells over a 3 m screened interval at a depth of approximately 8 m.

As part of this project, downhole radar, cross-well radar tomography and vertical radar profiling (VRP) data sets were acquired for subsequent interpretation and

Final copy as submitted to *Leading Edge* for publication as: Witten, A., and Lane, J.W., Jr., 2003, Offset vertical radar profiling: *Leading Edge*, v. 22, no. 11, p. 1070-1076.

processing. Here, the VRP aspect of the study is presented. In VRP, a receiving antenna is moved vertically in a well for an array of transmitting antenna positions arranged along a line on the ground surface radially outward from the receiver well. Many of the wells in the cluster were used for this purpose in the study. Unlike the more traditional reflection-based radar data, VRP is almost impossible to directly interpret. The are a number ways to reconstruct images of spatial variations in wave speed or attenuation and the one selected for implementation here is diffraction tomography (Devaney, 1984). The following section presents an overview of the diffraction tomography algorithm for VRP, followed by a description of data acquisition, processing steps and the imaging results.

Diffraction Tomography Imaging. In VRP, an antenna, either transmitting or receiving, is positioned on the ground surface some distance l_0 from the borehole. The opposite antenna is moved vertically in the borehole with data being acquired at some prescribed vertical interval Δz. For each measurement location l in the borehole, time samples are collected over some time window in time increments Δt. This acquisition geometry yields the equivalent of an array of antennas in the borehole and, by sequentially moving the surface antenna, a fully multistatic data set is developed similar to that used in offset vertical seismic profiling (VSP).

Diffraction tomography imaging algorithms have been developed for a variety of measurement configurations. All of these exploit the so called “generalized projection slice theorem”(GPST) that, in the frequency domain, relates the spatial Fourier transform of the acquired data to the spatial Fourier transform of the “object function” *O* which is defined to be one minus the square of the complex refractive index. In implementing

Final copy as submitted to *Leading Edge* for publication as: Witten, A., and Lane, J.W., Jr., 2003, Offset vertical radar profiling: *Leading Edge*, v. 22, no. 11, p. 1070-1076.

diffraction tomography in VRP or VSP, the measurements are two-dimensional and a function of the surface antenna position, l_0, and borehole antenna position, l. These two arrays define a vertical cross-section immediately below the antenna line l_0 and here this is considered the *(x,z)* plane. From such a set of measurements, imaging the out-of-cross-section region is impossible and it must be assumed that *O=O(x,z)*. For VSP using compressional (p) waves, the GPST is derived from the scalar wave equation through a deconvolution achieved by applying spatial Fourier transforms with respect to both the source location, l_0 and receiver location l (Devaney, 1984). When applied in this manner, the spatial Fourier transform decomposes a wave field into a superposition of plane waves propagating in various directions. Data derived from wave-based measurements can be thought of as a collection of experiments, where each experiment is represented by a particular pairing of source and receiver. The Fourier transform with respect to source location decomposes the wave created from an array of source locations into illuminating plane waves. This is commonly known as a "slant stack." Similarly, the Fourier transform with respect to receiver location is a collection of scattered plane waves captured by the receiver array. In this manner, the GPST represents a new pairing that relates incident and scattered plane waves rather than individual source/receiver locations. The benefit of the GPST is that it can provide and analytic relationship between the received signal and the object function, *O*, that characterizes the spatial variations in wave speed.

A general form of the GPST is given by

$$\tilde{D}(\mu,\nu,k) = H^{-1}(\mu,\nu,k)\ \tilde{O}(\boldsymbol{K}) \qquad (1)$$

Final copy as submitted to *Leading Edge* for publication as: Witten, A., and Lane, J.W., Jr., 2003, Offset vertical radar profiling: *Leading Edge*, v. 22, no. 11, p. 1070-1076.

where $\tilde{D}$ and $\tilde{O}$ are spatial Fourier transforms of the data and the object function, respectively. In Eq. (1), it has been assumed the data in the time domain has been temporally Fourier transformed and that one frequency ω has been selected for image reconstruction so that, for a background wave speed c_0, the background wavenumber is $k = \omega / c_0$. The Fourier transform parameters μ and ν are related to the direction of propagation of the incident and scattered plane waves. The filter H^{-1} and the two-dimensional *(x,z)* wave vector ***K*** are specific to a measurement geometry.

The GPST, as given by Eq. (1), can be rewritten as

$$\tilde{O}(\mathbf{K}) = H(\mu,\nu,k)\ \tilde{D}(\mu,\nu,k) \qquad (2)$$

where H^{-1} is the inverse of H which is the mathematical representation of a holographic lens. Equation (2) relates two spatial Fourier transforms and, as such, the right-hand side of this equation can be inverted by standard numerical methods to produce the final result of the diffraction tomography algorithm, an image of spatial variations in the object function or wave speed.

In Eq. (1), it has been assumed the data in the time domain has been temporally Fourier transformed and that one frequency ω_0 has been selected for image reconstruction so that, for a background wave speed c_0, the background wavenumber is $k = \omega_0 / c_0$. The incident field u_0 that would be received in the absence of variations in wave speed, $O = 0$, has been subtracted from the acquired data u and D represents a form of the perturbed wave field that depends on the weak scattering approximation used in the reconstruction. The Born approximation (Born and Wolf, 1980) is most commonly used and it assumes that scattering objects are manifested in the acquired data as a small additive perturbation on the incident field u_0. The weak scattering approximation used here is the Rytov

Final copy as submitted to *Leading Edge* for publication as: Witten, A., and Lane, J.W., Jr., 2003, Offset vertical radar profiling: *Leading Edge*, v. 22, no. 11, p. 1070-1076.

(Devaney, 1981) where the scattering objects are represented in the data as a small multiplicative correction to u_0 in the form $D = u_0 \ exp\ (\psi)$, where ψ is referred to as the complex phase.

A similar form of the GPST can be derived for VRP; however, this is based on a vector form of the wave equation that includes the diadic Green's function $\mathbf{G}$ rather than the scalar Green's function. The actual GPST is based on a scalar wave equation where the transmitting and receiving antenna polarizations are defined by the unit vectors e_T and e_R, respectively and the scalar form of the Green's function becomes $e_R \cdot \mathbf{G} \cdot e_T$ (Witten, et. al., 1996). This introduces antenna polarization into Eq. (2) through H.

Data Acquisition and Processing. There are number of wells at the site that have been used for tracer injection and monitoring of its movement within the shallow unconfined aquifer. Some of these wells were used as a host for the receiving antenna in a sequence of VRP experiments. The relative well locations are shown in Fig. 1 and those that were used in the VRP data acquisition are identified as **I1**, **I2**, **I3**, **M1**, and **M7**. For each receiver well, a number of source lines $\mathbf{l}_0$ were established radially outward where the length and orientation of each line is indicated on Fig 1. With the transmitting antenna fixed at an initial position near the receiver well for a given line, the receiving antenna was moved vertically in the borehole acquiring 512 time samples over a 500 ns time window. Such traces were acquired at a uniform receiver spacing of 0.2 m. This procedure was repeated as the source location was sequentially moved at a fixed interval of 0.5 m along each source line. Source line lengths varied between 4 and 8.5 m and the

Final copy as submitted to *Leading Edge* for publication as: Witten, A., and Lane, J.W., Jr., 2003, Offset vertical radar profiling: *Leading Edge*, v. 22, no. 11, p. 1070-1076.

antennas employed have a 100 MHz center frequency. The complete data set for each source line is used to reconstruct a single image of a vertical cross-section below that particular line.

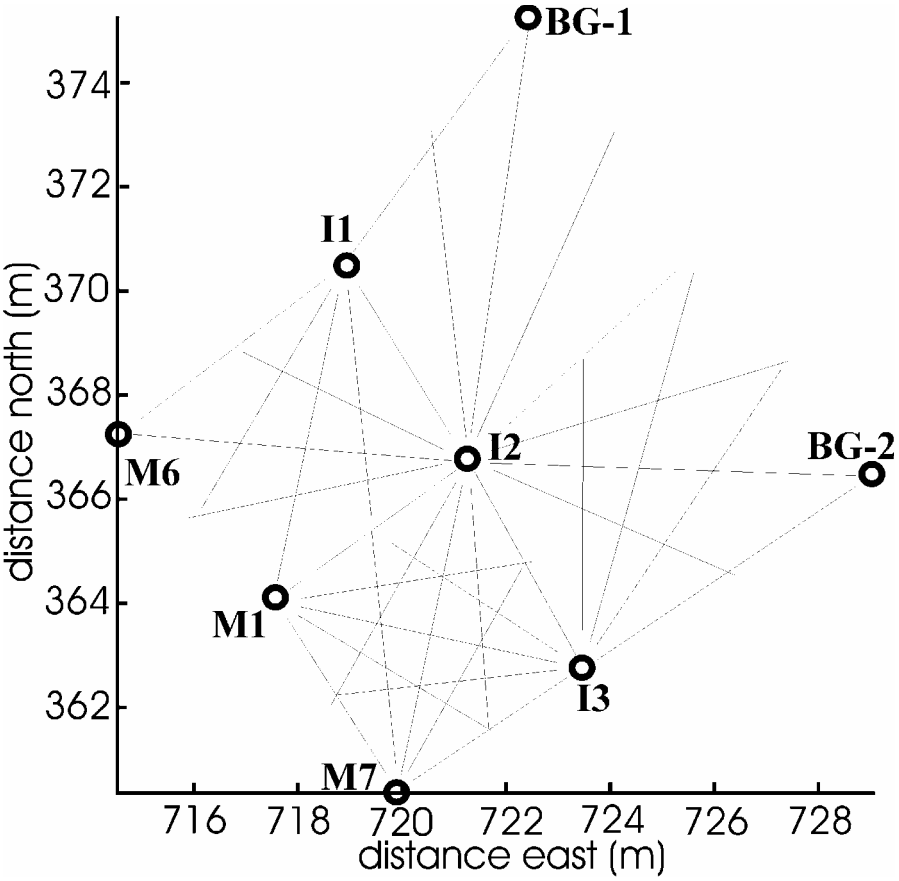

Figure 1: Illustration showing the location of wells (circles) and the VRP source lines used for data acquisition.

The diffraction tomography-based VRP processing described in the previous section is implemented at fixed frequency. Consequently, the first processing step is to perform a temporal Fourier transform and select the component at a desired frequency, ω.

Normally, this done by inspection of the power spectra for data acquired over any source line and selecting the highest possible frequency where there is significant power. Since image resolution is frequency-dependent, the best realizable image resolution is obtained at the highest frequency. As discussed in the previous section, images can be reconstructed using either the Born or Rytov approximation. The algorithm is the same for both; however, the definition of the reduced data *D* depends on the particular approximation invoked. Here, the Rytov approximation is used where *D* depends on the complex phase ψ. The imaginary part of the complex phase is the oscillatory component and the real part is the log amplitude. An additional processing step, phase unwrapping, is required to implement the Rytov approximation. This results from the fact that only the principal value, ψ^p of the phase can directly be computed and this is constrained to be in the interval $(-\pi,\pi)$. The principal value of the phase is the fractional part of the total number of wave cycles over the travel distance between source and receiver. One element of phase unwrapping is the determination of the integer number of cycles, i.e., the addition of $2\pi n$ to the principal value where *n* must be estimated. It is this complicating aspect of phase unwrapping that makes the Rytov approximation less appealing than the Born approximation; however, the Rytov can yield superior images. To estimate *n*, the recorded time series at the shallowest receiver location is inspected for each source location and, for each of these time series, a first arrival time, τ is selected. The integer *n* is then computed such that the real part of the phase, $\psi_R = \psi^p + 2\pi n$ is within $+/-\pi$ of $\omega\tau$ (Witten and King, 1990). The last step in the phase unwrapping is to add $+/-2\pi$ to successively deeper receiver location such that there is smooth variation in phase with receiver depth. This element of phase unwrapping is automatic and is quite reliable

provided that the interval between successive receiver positions is substantially less than one wavelength. This is a motivation for employing the 0.2 m receiver spatial sampling.

The only additional input for imaging is the specification of the background wave speed c_0 that is required for the background wavenumber $k = \omega_0 / c_0$ that appears in Eqs. (1) and (2). For this purpose, travel time τ for each source-to-receiver pair can approximately be related to the real part of the phase by $\omega_0 \tau \sim \psi_R$. It is further assumed that each ray path follows a straight line over a distance L defined by each source receiver separation. For each source/receiver pair, the straight ray estimated wave speed is simply L/τ. The background wave speed, c_0 is taken as the average over all ray-averaged wave speeds. This typically yields reasonable background wave speed; however, this value can be varied to refine the images.

Imaging Results. The complex phase consists of a real part, ψ_R, discussed in the above section and an imaginary part that is the log amplitude. The imaginary part of the complex phase can be directly computed from the amplitude of the temporal Fourier transform of the data so that, after phase unwrapping, the frequency domain input data D is fully known. For this application, images are reconstructed using ψ_R only, making the input amplitude independent. This eliminates any unquantified amplitude variations that can occur from both local changes in antenna coupling and unanticipated variations in antenna polarization. For traditional surface reflection based radar measurements over a horizontal reflecting surface, there will be a measured reflected signal for co-polarized transmitting and receiving antennas but no measured response for cross-polarized antennas. In this situation, slight random variations in antenna polarization will produce

Final copy as submitted to *Leading Edge* for publication as: Witten, A., and Lane, J.W., Jr., 2003, Offset vertical radar profiling: *Leading Edge*, v. 22, no. 11, p. 1070-1076.

random variations in the received signal that are unrelated to subsurface structure. Similar effects of unwanted antenna polarization can occur in VRP measurements and explicity appear in the forward model, Eq. (1), through the filter H^1. Since the real part of the phase, ψ_R is related to travel time, it would appear that neglecting amplitude would only admit the possibility of reconstructing images of spatial variation in wave speed but not attenuation. While this is the case for straight ray based imaging, it is not true for diffraction tomography. In diffraction tomography, the wave equation is inverted subject only to a weak scattering approximation. The effects of amplitude and phase are individually blended by the convolution of the Green's function with the complex object function O. Through this mechanism, both the real and imaginary parts of ψ contain information about spatial variations in both wave speed and attenuation. It has been shown that images of both wave speed and attenuation can be reconstructed from the real or imaginary parts of ψ (Devaney, 1989; Witten and Molyneux, 1992).

The purpose of this VRP imaging study is to characterize the spatial distribution of a vegetable oil tracer in a shallow unconfined aquifer. For each source line (Fig. 1), a two-dimensional vertical cross-section below the line is imaged. The vertical extent of the image spans the vertical range of receiving antennas in the well which, for these measurements, is over a depth interval from 1 to 12.5 m. The horizontal extent of the imaged cross-section is arbitrary; however, increasing this beyond the span of the source line locally degrades the image quality by limiting the range of illumination directions (views). For many of the lines, the horizontal extent of the imaged region was limited to distances from the receiver well that are somewhat less than the length of the source because of signal attenuation over the longer propagation distances. Using many source

Final copy as submitted to *Leading Edge* for publication as: Witten, A., and Lane, J.W., Jr., 2003, Offset vertical radar profiling: *Leading Edge*, v. 22, no. 11, p. 1070-1076.

lines from a number of receiver wells (Fig. 1), it is possible to create a composite three-dimensional "picture" of the tracer plume.

At the time of the vegetable oil injection, the water table was about 8 m below the ground surface and the tracer was injected through a screened interval between 12.2 and 15.2 m below the ground surface. The site is adjacent to the Mississippi River and the hydraulic gradient is largely controlled by the water level in the river. This can produce groundwater flow that varies in both magnitude and direction over time and the resulting advection of the tracer can cause the plume to have a complicated spatial structure.

The three main features anticipated in the images are dry or partial saturated near-surface soils that are characterized by a high wave speed and low attenuation, the unconfined aquifer characterized by a low wave speed and high attenuation, and the plume within the aquifer characterized by a high wave speed and low attenuation. These differences in characteristics suggest that all could be resolved by reconstructing images of either wave speed, the real part of *O*, or attenuation, the imaginary part of *O* and, as noted above, both can be reconstructed from phase only (ψ_R) information. For a number of source lines, both speed and attenuation images were generated and, for each cross-section, they provided similar results with the wave speed images being slightly superior to those for attenuation. For this reason, the effort focused on imaging the real part of *O*. All images were reconstructed at a frequency of 30 MHz that is much lower than the 100 MHz center frequency of the antennas. The reason for this is that to produce a reasonably good image of the plume it is necessary to have sources deployed along as long a line as possible and there is preferential attenuation of the high frequencies components from the distant sources as the wave propagates through the conductive aquifer.

Final copy as submitted to *Leading Edge* for publication as: Witten, A., and Lane, J.W., Jr., 2003, Offset vertical radar profiling: *Leading Edge*, v. 22, no. 11, p. 1070-1076.

A total of 47 cross-sectional images were reconstructed from that number of source lines radially outward from 8 receiver wells. Examples of two of these images are presented as false color in Fig. 2 where color variations from blue to red are associated with a range of electromagnetic waves speeds between 0.08 and 0.14 m/ns. Both images show a similar vertical structure exhibiting a high shallow wave speed (red) of the dry to partially saturated soil in the upper 4 m with low wave speed below (blue) indicative of the unconfined aquifer. Both images exhibit a wave speed increase (yellow and red) within the aquifer that is presumably a manifestation of the vegetable oil plume. The plume is shallower in Fig. 2b and thus is somewhat better defined. In all images, it was not possible to image the lower boundary of the plume because of the limited well depth that was accessible to the receiving antenna. The reason that the bottom of the relatively dry soil appears at a depth 4 m in the images while the water table is at an approximate depth of 8 m is that there is a transition in soil moisture content that is represented by a wave speed gradient in the imaged results. Furthermore, because of the relatively low frequency employed in image reconstruction, this transition is blurred.

Final copy as submitted to *Leading Edge* for publication as: Witten, A., and Lane, J.W., Jr., 2003, Offset vertical radar profiling: *Leading Edge*, v. 22, no. 11, p. 1070-1076.

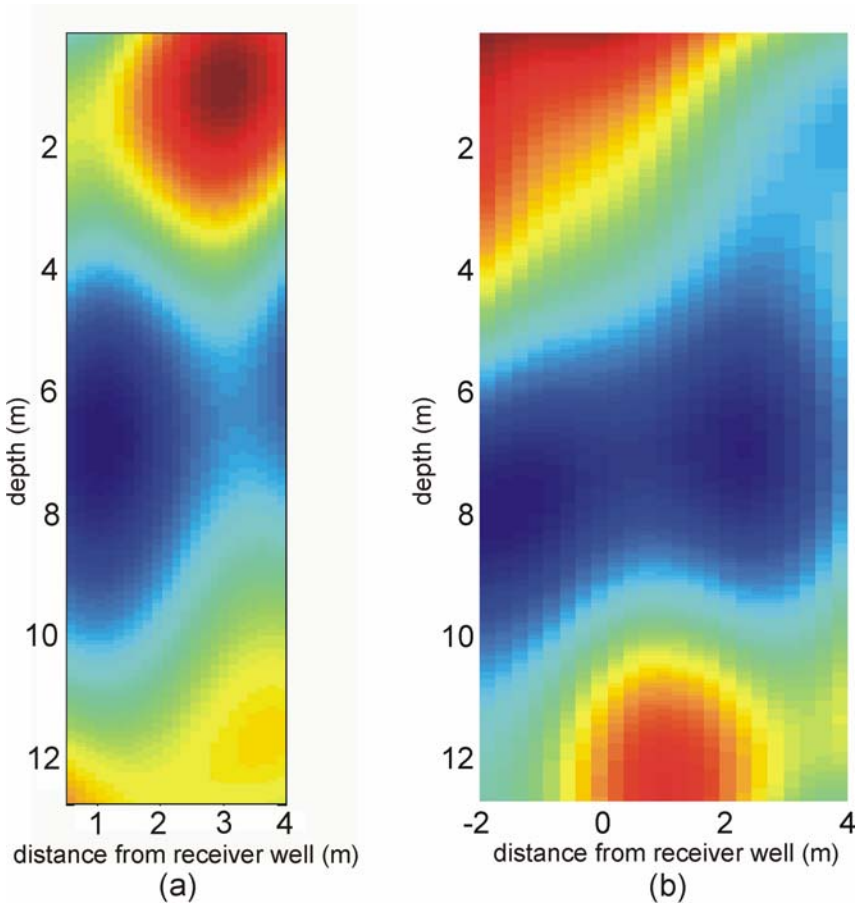

Figure 2: False color images of the spatial variation in wave speed for two of the 47 reconstructed vertical cross-sections.

In both images, the boundary between dry and saturated soil, although imprecise, should be close to horizontal. Part of the apparent tilting is associated with the limited views imposed by the relatively short source lines. Image resolution is wavelength dependent and for the 30 MHz frequency used for image reconstruction the wavelength is about 3 m. Part of the tilt of the top of the aquifer in Fig. 2 is a result of blurring where this interface appears as a subdued replication of the plume.

In the absence of absolute ground truth, image fidelity can be assessed by comparing variations among imaged cross-sections. There are a number of replicated

Final copy as submitted to *Leading Edge* for publication as: Witten, A., and Lane, J.W., Jr., 2003, Offset vertical radar profiling: *Leading Edge*, v. 22, no. 11, p. 1070-1076.

cross-sections that are images resulting from near identically located source lines for receivers emplaced in two different wells (Fig. 1). Apart from aperture-induced tilting, as discussed above, all such images compared favorably. Although a plume is evidently presents in the two images shown in Fig. 2, this is not the case for all imaged cross-section. Many of these clearly show the aquifer with no area of high wave speed present. Since the plume or plumes have some non-random structure, there should be relatively smooth transitions between where plumes are present and where they are absent. This was consistently the case for all the images.

To visualize the results in three dimensions, each cross-sectional image is horizontally rotated such that for distance along the source line l_0, (east, north) coordinates are assigned consistent with the source line map (Fig. 1). In this form, the information from all imaged cross-sections is interpolated onto a regular three-dimensional grid for subsequent display. For displaying the spatial extent of the plume, an effect visualization method is to create a surface in three dimensions that encloses a volume of constant reconstructed wave speed. Such an isosurface plot is shown in Fig. 3 where the bounding value is a wave speed of 0.12 m/ns. Since both the unsaturated near-surface soil and the vegetable oil plume both have comparably high wave speeds, the imaged volume is displayed only for depths greater than 5 m so as to eliminate the solid "lid" on the image. Two plumes are clearly visible; one from injection well **I1** and the other from injection well **I2**. Well **I3** was also used for injection; however, the down-gradient region from this plume is outside of the imaged volume.

Final copy as submitted to *Leading Edge* for publication as: Witten, A., and Lane, J.W., Jr., 2003, Offset vertical radar profiling: *Leading Edge*, v. 22, no. 11, p. 1070-1076.

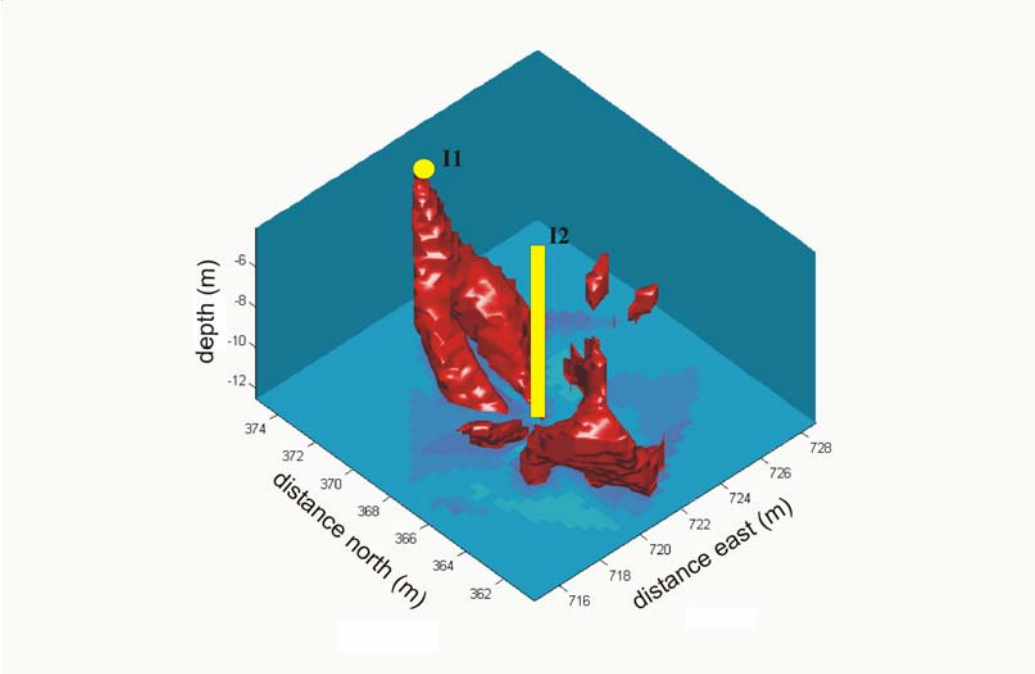

Figure 3: Isosurface plot showing the spatial distribution of high wave speed plumes.

The plume from **I1**, which is considerable larger than that from **I2**, shows a bifurcation that could be an artifact of interpolation, and seems to have migrated vertically within the annulus surrounding the well. The smaller plume from **I2** has advected away from the injection point.

Conclusions. Diffraction tomography imaging was applied to VRP data acquired by vertically moving a receiving antenna in a number of wells. This procedure simulated a vertical downhole receiver array. Similarly, a transmitting antenna was sequentially moved along a series of radial lines extending outward from the receiver wells. This provided a sequence of multistatic data sets and, from each data set, a two-dimensional vertical cross-sectional image of spatial variations in wave speed was reconstructed.

Final copy as submitted to *Leading Edge* for publication as: Witten, A., and Lane, J.W., Jr., 2003, Offset vertical radar profiling: *Leading Edge*, v. 22, no. 11, p. 1070-1076.

Each two dimensional image revealed relatively dry soil characterized by a high wave speed to a depth of about 4 m. Below this partially saturated soil layer, a gradient in wave speed was revealed indicating the expected transition to an unconfined aquifer. The lowest reconstructed wave speed appeared below the transition indicating the presence of the aquifer. Isolated region of high wave speed appeared embedded in the aquifer in many of the cross-section and these are suggestive of the presence of vegetable oil plumes. Collectively, these two-dimensional images provide a three-dimensional picture of the spatial extent of the plumes. This fact becomes more evident when the individual cross-sectional images are integrated into a three-dimensional display. In this manner of presentation, two high wave speed plumes are clearly identifiable and are both migrating southward away from the injection points and approximately parallel to the downstream flow of the nearby Mississippi River.

VRP imaging can be beneficial for assessing the efficacy of in situ bio remediation by providing information on the spatial distribution of features of interests, such as contaminants or injected tracers, between monitoring wells. For this to be effective, there must be sufficient wave speed contrast between the material of interest and its host. For the vegetable oil plumes mapped here, there is a strong wave speed contrast. High frequency electromagnetic waves can be attenuated by geologic material. The surficial sandy soils encountered at the subject site are not highly attenuating in their dry state; however, attenuation typically increases with moisture content. This can limit the spatial extent of VRP imaging particularly when the objective is to map groundwater additives. In such cases, the most important ray paths are those that pass through the plume and these must necessarily pass through the attenuating aquifer as well. The well

geometry for the case considered here is well suited for VRP measurements because closely spaced receiver wells were available. This allowed the use of many relatively short source lines such that manageable propagation distances could be achieved. Still, for a maximum receiver depth of about 13 m, horizontal source offsets were limited to about 8 m. Had the aquifer of interest been deeper it is likely that VRP imaging could not have been applied. Under these conditions, cross-borehole measurements would be preferable.

Suggested Reading

Born, M. and Wolf, E., 1980, Principles of Optics, Pergamon Press, Oxford.

Devaney, A.J., 1981, Inverse scattering theory within the Rytov approximation: Optics Letters, **6**, 376-381.

Devaney, A.J., 1984, Geophysical diffraction tomography: IEEE Trans. Geosci. and Remote Sensing, **GE-22**, 3-13.

Devaney, A.J., 1989, Structural determination from intensity measurements in scattering experiments: Appl. Phys. Lett., **62**, 2385-2388.

Witten, A.J. and King, W.C., 1990, Geophysical imaging with backpropagation and the zeroth-order phase approximation: Geophysical Research Letters, **17**, 673-676.

Witten, A.J. and Molyneux, J.E., 1992, Geophysical diffraction tomography: validity and implementation, in Geophysical Inversion, J. Bee Bednar, R.H. Stolt, A.B. Weglein, Eds., Siam, Philadelphia, 354-369.

Witten, A.J., Schatzberg, A., and Devaney, A.J., 1996, Vector radar wave diffraction tomography maximum likelihood estimation: Journal of Environmental and Engineering Geophysics, **0**, 91-104.

Final copy as submitted to *Leading Edge* for publication as: Witten, A., and Lane, J.W., Jr., 2003, Offset vertical radar profiling: *Leading Edge*, v. 22, no. 11, p. 1070-1076.